Available online at www.sciencedirect.com
SCIENCE DIRECT®

Journal of the European Ceramic Society 26 (2006) 233–246

www.elsevier.com/locate/jeurceramsoc

Phase diagram of the ZrO_2–Gd_2O_3–Al_2O_3 system

S. Lakiza[a,b], O. Fabrichnaya[b,*], Ch. Wang[b], M. Zinkevich[b], F. Aldinger[b]

[a] *Frantsevich Institute of Materials Science Problems, Kiev, Ukraine*
[b] *Max-Planck-Institute für Metallforschung, Pulvermetallurgisches Laboratorium, Heisenbergstr 5, 70569 Stuttgart, Germany*

Received 21 August 2004; received in revised form 15 November 2004; accepted 21 November 2004
Available online 26 January 2005

Abstract

Isothermal sections of the phase diagram for the ZrO_2–$GdO_{3/2}$–$AlO_{3/2}$ system have been constructed based on experimental phase equilibrium data at 1250 and 1650 °C. They are in a good agreement with calculations which have also been performed in the present study. The liquidus and solidus surfaces have been experimentally determined. The temperature of the eutectic reaction liquid = Al_2O_3 + fluorite + $GdAlO_3$ was measured using differential thermal analysis (DTA) to be 1662 °C. The liquidus surface calculated in this work using a non-zero ternary interaction parameter in the liquid phase agrees with the experimental data. A thermodynamic description of the ZrO_2–$GdO_{3/2}$–$AlO_{3/2}$ system based on an ionic sublattice model for the solid and liquid phases consistent with the experimental data has been derived.

Keywords: ZrO_2–Gd_2O_3–Al_2O_3; Microstructure-final; X-ray methods; Thermodynamic modelling; Phase equilibria

1. Introduction

The yttria-stabilised zirconia (YSZ) system is a most commonly used thermal barrier coating (TBC). Co-doping of YSZ with Gd enhances its thermal insulation properties without loss of thermal stability.[1] The pyrochlore structure formed in the ZrO_2–Gd_2O_3 system has also a lower thermal conductivity than YSZ.[2,3] These materials (Gd co-doped YSZ and pyrochlore) are therefore candidates for advanced TBC. Chemical insulation of the bond coat is provided by Al_2O_3 (thermally grown oxide, TGO). Phase relations in the ZrO_2–Gd_2O_3–Al_2O_3 system are important to understand interactions between TBC and TGO. The phase diagram of the ZrO_2–Gd_2O_3–Al_2O_3 system is necessary for a successful materials development for thermal barrier coating.

The phase diagrams of the bounding binary systems have been examined in some detail.[4–9] ZrO_2 occurs in three polymorphic modifications: monoclinic (M), tetragonal (T), and cubic fluorite-like (F). Gd_2O_3 crystallises in five polymorphic forms: low-temperature cubic (C), monoclinic B (B), hexagonal A (A), hexagonal H (H) and X-phase (X). The Al_2O_3–ZrO_2 system is dominated by an eutectic reaction between T and corundum (AL) and its phase diagram is described elsewhere.[4] The ZrO_2–Gd_2O_3 system reveals limited mutual solubility of the components in the solid state.[5] A superstructure compound $Gd_2Zr_2O_7$ (Pyr) of a pyrochlore type with rather wide homogeneity range was found in this system at temperatures up to 1540 °C. The liquidus contains eutectic L $\rightleftarrows$ F + H (2260 °C, 87 mol% $GdO_{3/2}$) and metatectic (2375 °C, 95 mol% $GdO_{3/2}$) points. The F $\rightleftarrows$ T $\rightleftarrows$ M phase transformations of ZrO_2 and A $\rightleftarrows$ B $\rightleftarrows$ C phase transformations of Gd_2O_3 occur in the solid state and do not display on the liquidus curves. The Al_2O_3–Gd_2O_3 system includes two compounds: $GdAlO_3$ (GAP) congruently melting at 2050 °C with perovskite-like structure and $Gd_4Al_2O_9$ (GAM) with monoclinic structure.[6–9] Literature data about the melting character of GAM are contradictory.[6–7,9] No homogeneity range was found for the GAP and GAM phases in the Al_2O_3–Gd_2O_3 system. The phase transformations of Gd_2O_3 X $\rightleftarrows$ H $\rightleftarrows$ A $\rightleftarrows$ B display on the liquidus curve as metatectic points at 2360 °C and 98 mol% Gd_2O_3, 2200 °C and 89 mol% Gd_2O_3, and 2170 °C and 87 mol% Gd_2O_3, respectively. The phase transformation of Gd_2O_3 B $\rightleftarrows$ C takes place at 1200 °C and does not display on the liquidus of the Al_2O_3–Gd_2O_3 system. The phase diagram of the ZrO_2–Gd_2O_3–Al_2O_3 system

* Corresponding author. Tel.: +49 711 689 3106; fax: +49 711 689 3131.
E-mail address: fabri@mf.mpg.de (O. Fabrichnaya).

0955-2219/$ – see front matter © 2004 Elsevier Ltd. All rights reserved.
doi:10.1016/j.jeurceramsoc.2004.11.011

has not been experimentally investigated so far except for the isothermal section at 1473 K.[10]

Thermodynamic descriptions for the binary systems are available. The thermodynamic parameters were assessed for the ZrO_2–Gd_2O_3 system,[11] for the Gd_2O_3–Al_2O_3 system[8] and for the ZrO_2–Al_2O_3 system.[12–14] However, the liquid phase was described by a substitutional model in the ZrO_2–Gd_2O_3 system, by a quasichemical model in the Gd_2O_3–Al_2O_3 system, and by an ionic, associate and quasichemical model in the ZrO_2–Al_2O_3 system. Different models were also applied to the solid phases in the binary systems. Therefore, since the liquid phases are described by different models, the available descriptions of the binary systems cannot be combined to create a database for the ternary system. New calorimetric data have appeared recently,[15–18] which were not available for the previous assessments. A thermodynamic assessment of the ternary system ZrO_2–Gd_2O_3–Al_2O_3 has not been available.

The aim of this work is to study phase relations in the ZrO_2–Gd_2O_3–Al_2O_3 system experimentally and to derive a thermodynamic description of this system using the obtained data. The isothermal sections at 1250 and 1650 °C, the tentative liquidus and solidus projections on the concentration triangle, and the Scheil reaction scheme are constructed. The obtained experimental data are used to derive a thermodynamic database for this system.

2. Experimental details

Specimens were obtained from pure oxides and from more complex precursors. In the first case powders of alumina (99.9%; Donetskij zavod khimreaktiviv, Donetsk, Ukraine), zirconia (99.99%; Donetskij zavod khimreaktiviv) and gadolinia (99.99%; Strem Chemicals) were used as raw materials. The appropriate quantities of oxides were mixed in an agate mortar with ethanol, dried and isostatically pressed into pellets 5 mm in diameter and 5 mm in height.

In the second case, powders of $Al(NO_3)_3{\cdot}9H_2O$ and $ZrO(NO_3)_2{\cdot}2H_2O$ with purity of 99.9% (Donetskij zavod khimreaktiviv) and Gd_2O_3 of 99.99% (Strem Chemicals) were used. Both salts were dissolved separately in distilled water and the yields of pure oxides in g/ml were determined. The appropriate quantity of gadolinia was dissolved in diluted nitric acid and the Al^{3+} and Zr^{4+} solutions were added. The received three-component solution was dried, and the residual calcined at 600 °C in air. The obtained powder was pressed into pellets 5 mm in diameter and 5 mm in height. The specimens compositions were selected on bisector 50 mol% Al_2O_3–50 mol% ZrO_2 (50A·50Z) − Gd_2O_3 and based on the results of the liquidus surface calculation. Compositions of some additional samples were chosen during localization of the ternary eutectic points.

The specimens were investigated by X-ray diffraction (XRD; Model D-5000, Siemens AG, Karlsruhe, Germany), differential thremal analysis (DTA; Model STA 502, Bähr-Thermoanalyse, Hüllhorst, Germany) in air at temperatures up to 1700 °C, petrographic (MIN-8 optical microscope, LOMO, St. Petersburg, Russia) and microstructural phase (Model DSM-982 Gemini, Karl Zeiss Inc., Oberkochen, Germany) analysis. For the constructing of isothermal sections precursor derived samples were annealed at 1250 and 1650 °C for the time necessary to attain equilibrium, established by the absence of further changes on XRD patterns. Other samples were fired at 1250 °C in air for 6 h, melted in molybdenum crucibles in a furnace with H_2 environment and annealed at 1650 °C for 1 h. Samples for microstructural phase analysis were obtained by crystallization from melt.

3. Modelling

The Calphad method[19] based on computer coupling of thermochemistry and phase diagram considerations is used in this study to assess thermodynamic parameters in binary and ternary systems. The phases, which are stable in the system ZrO_2–Gd_2O_3–Al_2O_3 and thermodynamic models used to describe them are shown in Table 1. The liquid phase is described by a two-sublattice ionic liquid model. Most of the solid phases are described by the compound energy formalism;[20] the remaining solid phases are treated as stoichiometric compounds. No ternary compounds were found in the system. This circumstance allows us to make extrapolation from binary systems to ternary system.

The thermodynamic parameters for the similar system ZrO_2–Y_2O_3–Al_2O_3 were derived by Fabrichnaya et al.[21] where cubic phases with fluorite and bixbyite structures were considered as one phase having a miscibility gap. In the present study, the fluorite and cubic Gd_2O_3 solid solutions are described by different models. This is more consistent with the crystal structure of these phases. The phase with fluorite structure can be described by two sublattices. One is filled by Zr^{4+} and Gd^{3+} cations. The other one contains disordered oxygen anions and vacant positions $(Zr^{4+}, Gd^{3+})(O^{2-}, Va)_2$. The vacancies in the C phase with bixbyite structure are ordered and the anionic sublattice is subdivided into two sublattices—one completely filled by oxygen anions and another one partly vacant $(Gd^{3+}, Zr^{4+})_2(O^{2-})_3(O^{2-}, Va)$. The structure of the pyrochlore phase is well known.[22–24] It contains five crystallographically different sublattices with strong preference of cations and anions to each sublattice:

$$(Gd^{3+},\ Zr^{4+})_2(Zr^{4+},\ Gd^{3+})_2(O^{2-},\ Va)_6(O^{2-})(Va,\ O^{2-}).$$

The Gibbs energy of a solution phase with mixing in two sublattices (i.e. fluorite, tetragonal phase, C, H) is expressed as:

$$\Delta G = \sum_i \sum_j Y_i^s Y_j^t G_{i,j} + RT \sum_s \alpha_s \sum_i Y_i^s \ln Y_i^s + \Delta G^{\text{ex}}$$

where Y_i^{s} is the mole fraction of a constituent i in sublattice s, α_s is the number of sites on sublattice s per mole of formula unit of phase and ΔG^{ex} is the excess Gibbs energy of mixing

Table 1
Thermodynamic parameters

Phase/temperature range	Model/parameter
Fluorite (F)	$(Al^{3+}, Gd^{3+}, Zr^{4+})_2(O^{2-}, Va)_4$
298.15–6000	$^{0}G^{F}(Zr^{4+}:O^{2-}) - 2\mathrm{HSERZr} - 4\cdot\mathrm{HSERO} = 2\mathrm{GZRO2C}$
298.15–6000	$^{0}G^{F}(Zr^{4+}:Va) - 2\mathrm{HSERZr} = 2\mathrm{GZRO2C} - 4\mathrm{GHSEROO}$
298.15–6000	$^{0}G^{F}(Gd^{3+}:O^{2-}) - 2\mathrm{HSERGd} - 4\mathrm{HSERO} = \mathrm{GGD2O3L} + \mathrm{GHSEROO} + 28.818016T - 16929.8$
298.15–6000	$^{0}G^{F}(Gd^{3+}:Va) - 2\mathrm{HSERGd} = \mathrm{GGD2O3L} - 3\mathrm{GHSEROO} + 28.818016T - 16929.7864$
298.15–6000	$^{0}G^{F}(Al^{3+}:O^{2-}) - 2\mathrm{HSERAl} - 4\mathrm{HSERO} = \mathrm{GCORUND} + \mathrm{GHSEROO} + 18.702165T + 100000$
298.15–6000	$^{0}G^{F}(Al^{3+}:Va) - 2\mathrm{HSERAl} = \mathrm{GCORUND} - 3\mathrm{GHSEROO} + 18.702165T + 100000$
298.15–6000	$^{0}L^{F}(Al^{3+}, Zr^{4+}:O^{2-}) = 7250.35$
298.15–6000	$^{0}L^{F}(Al^{3+}, Zr^{4+}:Va) = 7250.35$
298.15–6000	$^{0}L^{F}(Gd^{3+}, Zr^{4+}:O^{2-}) = -133013 - 14.5394T$
298.15–6000	$^{0}L^{F}(Gd^{3+}, Zr^{4+}:Va) = -133013 - 14.5394T$
298.15–6000	$^{1}L^{F}(Gd^{3+}, Zr^{4+}:O^{2-}) = 91084 - 35.8991T$
298.15–6000	$^{1}L^{F}(Gd^{3+}, Zr^{4+}:Va) = 91083.7478 - 35.8991T$
Tetragonal (T)	$(Al^{3+}, Gd^{3+}, Zr^{4+})_2(O^{2-}, Va)_4$
298.15–6000	$^{0}G^{T}(Zr^{4+}:O^{2-}) - 2\mathrm{HSERZr} - 4\mathrm{HSERO} = 2\mathrm{GZRO2}T$
298.15–6000	$^{0}G^{T}(Zr^{4+}:Va) - 2\mathrm{HSERZr} = 2\mathrm{GZRO2}T - 4\mathrm{GHSEROO}$
298.15–6000	$^{0}G^{T}(Gd^{3+}:O^{2-}) - 2\mathrm{HSERGd} - 4\mathrm{HSERO} = \mathrm{GGD2O3L} + \mathrm{GHSEROO} + 28.818016T - 16929.7864 + 10000$
298.15–6000	$^{0}G^{T}(Gd^{3+}:O^{2-}) - 2\mathrm{HSERGd} = \mathrm{GGD2O3L} - 3\mathrm{GHSEROO} + 28.818016T - 16929.7864 + 10000$
298.15–6000	$^{0}G^{T}(Al^{3+}:O^{2-}) - 2\mathrm{HSERAl} - 4\mathrm{HSERO} = \mathrm{GCORUND} + \mathrm{GHSEROO} + 18.702165T + 100000$
298.15–6000	$^{0}G^{T}(Al^{3+}:Va)\text{-}2\mathrm{HSERAl} = \mathrm{GCORUND} - 3\mathrm{GHSEROO} + 18.702165T + 100000$
298.15–6000	$^{0}L^{T}(Al^{3+}, Zr^{4+}:O^{2-}) = 18521$
298.15–6000	$^{0}L^{T}(Al^{3+}, Zr^{4+}:Va) = 18521$
298.15–6000	$^{0}L^{T}(Gd^{3+}, Zr^{4+}:O^{2-}) = 4749 - 42.0515T$
298.15–6000	$^{0}L^{T}(Gd^{3+}, Zr^{4+}:Va) = 4749 - 42.0515T$
Monoclinic (M)	$(Zr^{4+})_1(O^{2-})_2$
298.15–6000	$^{0}G^{M}(Zr^{4+}:O^{2-}) - \mathrm{HSERZr} - 2\mathrm{HSERO} = \mathrm{GZRO2M}$
Cubic_RE2O3 (C)	$(Gd^{3+}, Zr^{4+})_2(O^{2-})_3(O^{2-}, Va)_1$
298.15–6000	$^{0}G^{C}(Zr^{4+}:O^{2-}:O^{2-}) - 2\mathrm{HSERZr} - 4\mathrm{HSERO} = 2\mathrm{GZRO2C}$
298.15–6000	$^{0}G^{C}(Zr^{4+}:O^{2-}:Va) - 2\mathrm{HSERZr} - 3\mathrm{HSERO} = 2\mathrm{GZRO2C} - \mathrm{GHSEROO}$
298.15–6000	$^{0}G^{C}(Gd^{3+}:O^{2-}:O^{2-}) - 2\mathrm{HSERGd} - 4\mathrm{HSERO} = \mathrm{GGD2O3C} + \mathrm{GHSEROO}$
298.15–6000	$^{0}G^{C}(Gd^{3+}:O^{2-}:Va) - 2\mathrm{HSERGd} - 3\mathrm{HSERO} = \mathrm{GGD2O3C}$
298.15–6000	$^{0}L^{C}(Gd^{3+}, Zr^{4+}:O^{2-}:O^{2-}) = 7185 - 6.1943T$
298.15–6000	$^{0}L^{C}(Gd^{3+}, Zr^{4+}:O^{2-}:Va) = 7184.73281 - 6.1943T$
B_RE2O3 (B)	$(Gd^{3+}, Zr^{4+})_2(O^{2-})_3(O^{2-}, Va)_1$
298.15–6000	$^{0}G^{B}(Zr^{4+}:O^{2-}:O^{2-}) - 2\mathrm{HSERZr} - 4\mathrm{HSERO} = 2\mathrm{GZRO2C} + 50000$
298.15–6000	$^{0}G^{B}(Zr^{4+}:O^{2-}:Va) - 2\mathrm{HSERZr} - 3\mathrm{HSERO} = 2\mathrm{GZRO2C} - \mathrm{GHSEROO} + 50000$
298.15–6000	$^{0}G^{B}(Gd^{3+}:O^{2-}:O^{2-}) - 2\mathrm{HSERGd} - 4\mathrm{HSERO} = \mathrm{GGD2O3B} + \mathrm{GHSEROO}$
298.15–6000	$^{0}G^{B}(Gd^{3+}:O^{2-}:Va) - 2\mathrm{HSERGd} - 3\mathrm{HSERO} = \mathrm{GGD2O3B}$
298.15–6000	$^{0}L^{C}(Gd^{3+}, Zr^{4+}:O^{2-}:O^{2-}) = 74357 - 40.7987T$
298.15–6000	$^{0}L^{C}(Gd^{3+}, Zr^{4+}:O^{2-}:Va) = 74357 - 40.7987T$
A_RE2O3	$(Gd^{3+})_2(O^{2-})_3$
298.15–6000	$^{0}G^{A}(Gd^{3+}:O^{2-}:Va) - 2\mathrm{HSERGd} - 3\mathrm{HSERO} = \mathrm{GGD2O3A}$
Hexagonal_RE2O3	$(Gd^{3+}, Zr^{4+})_2(O^{2-})_3(O^{2-}, Va)_1$
298.15–6000	$^{0}G^{H}(Zr^{4+}:O^{2-}:O^{2-}) - 2\mathrm{HSERZr} - 4\mathrm{HSERO} = 2\mathrm{GZRO2C} + 50000$
298.15–6000	$^{0}G^{H}(Zr^{4+}:O^{2-}:Va) - 2\mathrm{HSERZr} - 3\mathrm{HSERO} = 2\mathrm{GZRO2C} - \mathrm{GHSEROO} + 50000$
298.15–6000	$^{0}G^{H}(Gd^{3+}:O^{2-}:O^{2-}) - 2\mathrm{HSERGd} - 4\mathrm{HSERO} = \mathrm{GGD2O3H} + \mathrm{GHSEROO}$
298.15–6000	$^{0}G^{H}(Gd^{3+}:O^{2-}:Va) - 2\mathrm{HSERGd} - 3\mathrm{HSERO} = \mathrm{GGD2O3H}$
298.15–6000	$^{0}L^{H}(Gd^{3+}, Zr^{4+}:O^{2-}:O^{2-}) = 397617 - 189.9203T$
298.15–6000	$^{0}L^{H}(Gd^{3+}, Zr^{4+}:O^{2-}:Va) = 397617 - 189.9203T$
X_RE2O3 (X)	$(Gd^{3+})_2(O^{2-})_3$
298.15–6000	$^{0}G^{X}(Gd^{3+}:O^{2-}:) - 2\mathrm{HSERGd} - 3\mathrm{HSERO} = \mathrm{GGD2O3X}$
Pyrochlore (Pyr)	$(Gd^{3+}, Zr^{4+})_2(Gd^{3+}, Zr^{4+})_2(O^{2-}, Va)_6\ (O^{2-})_1(O^{2-}, Va)_1$
298.15–6000	$^{0}G^{Pyr}(Zr^{4+}:Zr^{4+}:O^{2-}:O^{2-}:Va) - 4\mathrm{HSERZr} - 7\mathrm{HSERO} = \mathrm{GPYROZR} - \mathrm{GHSEROO}$
298.15–6000	$^{0}G^{Pyr}(Gd^{3+}:Zr^{4+}:O^{2-}:O^{2-}:Va) - 2\mathrm{HSERZr} - 2\mathrm{HSERGd} - 7\mathrm{HSERO} = \mathrm{GOPYRO}$
298.15–6000	$^{0}G^{Pyr}(Zr^{4+}:Gd^{3+}:O^{2-}:O^{2-}:Va) - 2\mathrm{HSERZr} - 2\mathrm{HSERGd} - 7\mathrm{HSERO} = \mathrm{GOPYRO} + 170978$
298.15–6000	$^{0}G^{Pyr}(Gd^{3+}:Gd^{3+}:O^{2-}:O^{2-}:Va) - 4\mathrm{HSERGd} - 7\mathrm{HSERO} = 2\mathrm{GOPYRO} - \mathrm{GPYROZR} + \mathrm{GHSEROO} + 170978$
298.15–6000	$^{0}G^{Pyr}(Zr^{4+}:Zr^{4+}:Va:O^{2-}:Va) - 4\mathrm{HSERZr} - \mathrm{HSERO} = 6\mathrm{GPYROGD} - 12\mathrm{GOPYRO} + 7\mathrm{GPYROZR}$ $- 7\mathrm{GHSEROO} - 1025867 + 134.8548T$

Table 1 (*Continued*)

Phase/temperature range	Model/parameter
298.15–6000	$^{0}G^{Pyr}(Gd^{3+}:Zr^{4+}:Va:O^{2-}:Va)$ − 2HSERZr − 2HSERGd-HSERO = 6GPYROGD − 11GOPYRO + 6GPYROZR − 6GHSEROO − 1025867 + 134.8548*T*
298.15–6000	$^{0}G^{Pyr}(Zr^{4+}:Gd^{3+}:Va:O^{2-}:Va)$-2HSERZr-2HSERGd-HSERO = 6GPYROGD − 11GOPYRO + 6GPYROZR − 6GHSEROO − 854889 + 134.8548*T*
298.15–6000	$^{0}G^{Pyr}(Gd^{3+}:Gd^{3+}:Va:O^{2-}:Va)$ − 4HSERGd − HSERO = 6GPYROGD − 10GOPYRO + 5GPYROZR − 5GHSEROO − 854889 + 134.8548*T*
298.15–6000	$^{0}G^{Pyr}(Zr^{4+}:Zr^{4+}:O^{2-}:O^{2-}:O^{2-})$ − 4HSERZr − 8HSERO = GPYROZR
298.15–6000	$^{0}G^{Pyr}(Gd^{3+}:Zr^{4+}:O^{2-}:O^{2-}:O^{2-})$ − 2HSERZr − 2HSERGd − 8HSERO = GOPYRO + GHSEROO
298.15–6000	$^{0}G^{Pyr}(Zr^{4+}:Gd^{3+}:O^{2-}:O^{2-}:O^{2-})$ − 2HSERZr − 2HSERGd − 8HSERO = GOPYRO + GHSEROO + 170977.794
298.15–6000	$^{0}G^{Pyr}(Gd^{3+}:Gd^{3+}:O^{2-}:O^{2-}:O^{2-})$ − 4HSERGd − 8HSERO = 2GOPYRO + 2GHSEROO − GPYROZR + 170977.794
298.15–6000	$^{0}G^{Pyr}(Zr^{4+}:Zr^{4+}:Va:O^{2-}:O^{2-})$ − 4HSERZr − 2HSERO = 6GOPYRO − 3GPYROGD2 − 2GPYROZR − 6GHSEROO + 174.454*T* + 710310.4428
298.15–6000	$^{0}G^{Pyr}(Gd^{3+}:Zr^{4+}:Va:O^{2-}:O^{2-})$ − 2HSERZr − 2HSERGd − 2HSERO = GOPYRO − 5GHSEROO + 98688.5403 + 134.8548*T*
298.15–6000	$^{0}G^{Pyr}(Zr^{4+}:Gd^{3+}:Va:O^{2-}:O^{2-})$ − 2HSERZr − 2HSERGd − 2HSERO = GOPYRO − 5GHSEROO + 269666 + 134.8548*T*
298.15–6000	$^{0}G^{Pyr}(Gd^{3+}:Gd^{3+}:Va:O^{2-}:O^{2-})$ − 4HSERGd − 2HSERO = 3GPYROGD2 − 4GOPYRO − 4GHSEROO + 2GPYROZR − 341956 + 95.2556*T*
Corundum (AL)	$(Al^{3+})_2(O^{2-})_3$
298.15–6000	$^{0}G^{AL}(Al^{3+}:O^{2-})$ − 2HSERAl − 3HSERO = GCORUND
GAM	$(Al^{3+})_2(Gd^{3+})_4(O^{2-})_9$
298.15–6000	$^{0}G^{GAM}(Al^{3+}:Gd^{3+}:O^{2-})$ = GCORUND + 2GGD2O3C − 65043 − 6.60296288*T*
GAP	$(Al^{3+})_1(Gd^{3+})_1(O^{2-})_3$
298.15–6000	$^{0}G^{GAM}(Al^{3+}:Gd^{3+}:O^{2-}) = -1832597.777 + 744.826493T - 122.614602T\ln(T) - 0.00651716289T^2 + 1521742.76/T$
GAG	$(Al^{3+})_5(Gd^{3+})_3(O^{2-})_{12}$
298.15–6000	$^{0}G^{GAG}(Al^{3+}:Gd^{3+}:O^{2-})$ = 2.5GCORUND + 1.5GGD2O3C − 119771 + 29*T*
IONIC_LIQ	$(Gd^{3+}, Zr^{4+})_P(O^{2-}, AlO_{3/2})_Q$
298.15–6000	$^{0}G^{L}(Zr^{4+}:O^{2-})$ = 2GZRO2L
298.15–6000	$^{0}G^{L}(Gd^{3+}:O^{2-})$ = GGD2O3L
298.15–6000	$^{0}G^{L}(AlO_{3/2})$ = 0.5GAL2O3_L
298.15–6000	$^{0}L^{L}(Zr^{4+}:O^{2-}, AlO_{3/2}) = 50000$
298.15–6000	$^{1}L^{L}(Zr^{4+}:O^{2-}, AlO_{3/2}) = -40000$
298.15–6000	$^{0}L^{L}(Gd^{3+}, Zr^{4+}:O^{2-}) = -57043.1057 - 48.6193813T$
298.15–6000	$^{1}L^{L}(Gd^{3+}, Zr^{4+}:O^{2-}) = 8116.08904$
298.15–6000	$^{0}L^{L}(Gd^{3+}:O^{2-}, AlO_{3/2}) = -43456.0044$
298.15–6000	$^{1}L^{L}(Gd^{3+}:O^{2-}, AlO_{3/2}) = 15239.3606$
298.15–6000	$^{0}L^{L}(Gd^{3+}, Zr^{4+}:O^{2-}, AlO_{3/2}) = 800709.258 - 360.029317T$
Functions	
298.15–2985	GZRO2M = $-1126367.62 + 426.0761T - 69.6218T\ln(T) - 0.00376567T^2 + 702910.0/T$
2986–6000	$-1145443.9237 + 567.31299T - 87.864T\ln(T) - 2.54642 \times 10^{33}T^{-9}$
298.15–1478	GZRO2*T* 298.15 $- 1117868.813 + 420.27778T - 69.6218T\ln(T) - 0.00376567T^2 + 702910.0/T + 4.589486 \times 10^{-21}T^7$
1478–2985	$-1121646.51 + 479.515703T - 78.10T\ln(T)$
2985–6000	$-1154030.428 + 568.38136T - 87.864T\ln(T) + 6.092955 \times 10^{33}T^{-9}$
298.15–1800	GZRO2C = $-1107276.18 + 416.6337865T - 69.6218T\ln(T) - 0.00376567T^2 + 702910.0/T + 1.920919 \times 10^{-21}T^7$
1800–2985	$-1113681.0 + 491.486437T - 80.0T\ln(T)$
2985–6000	$-1139763.268 + 563.059458T - 87.864T\ln(T) + 4.90732 \times 10^{33}\ T^{-9}$
298.15–2985	GZRO2L = $-1027958.268 + 390.79315T - 69.6218T\ln(T) - 0.00376567T^2 + 702910/T + 1.373457 \times 10^{-22}T^7$
2985–6000	$-1050128.04 + 533.11826T - 87.864T\ln(T)$
298.15–6000	GGD2O3C = $-1868253 + 660.409T - 119.206T\ln(T) - 6.4725 \times 10^{-3}T^2 + 780500/T$
298.15–6000	GGD2O3B = $-1859050 + 632.841T - 116.230099T\ln(T) - 0.00.647312337T^2 + 623563.197/T$
298.15–6000	GGD2O3A = GGD2O3B + 6300 − 2.57879667*T*
298.15–6000	GGD2O3H = GGD2O3B + 12380 − 5.02942137*T*
298.15–6000	GGD2O3X = GGD2O3B + 18987.5 − 7.52942137*T*
298.15–2698	GGD2O3L = $-1863570.5 + 777.80737T - 132.987058T\ln(T) - 0.0109082017T^2 + 1351313.97/T$
2698–6000	$-1940972 + 1239.328T - 191.476T\ln(T)$
298.15–600	GAL2O3_L = $-1607850.8 + 405.559491T - 67.4804T\ln(T) - 0.06747T^2 + 1.4205433 \times 10^{-5}T^3 + 938780/T$

Table 1 (*Continued*)

Phase/temperature range	Model/parameter
600–1500	$-1625385.57 + 712.394972T - 116.258T\ln(T) - 0.0072257T^2 + 2.78532 \times 10^{-7}T^3 + 2120700/T$
1500–1912	$-1672662.69 + 1010.9932T - 156.058T\ln(T) + 0.007091105T^2 - 6.29402 \times 10^{-7}T^3 + 12366650/T$
1912–2327	$29178041.6 - 168360.926T + 21987.1791T\ln(T) - 6.995529551T^2 + 4.10226192 \times 10^{-4}T^3 - 7.98843618 \times 10^9 T^{-1}$
2327–6000	$-1757702.05 + 1344.84833T - 192.464T\ln(T)$
298.15–600	GCORUND = $-1707351.3 + 448.021092T - 67.4804T\ln(T) - 0.06747T^2 + 1.4205433 \times 10^{-5}T^3 + 938780/T$
600–1500	$-1724886.06 + 754.856573T - 116.258T\ln(T) - 0.0072257T^2 + 2.78532 \times 10^{-7}T^3 + 2120700/T$
1500–6000	$-1772163.19 + 1053.4548T - 156.058T\ln(T) + 0.007091105T^2 - 6.29402 \times 10^{-7}T^3 + 12366650/T$
298.15–6000	GOPYRO = $-4163085.95 + 1416.11213T - 248.308422T\ln(T) + 1545056.71/T - 0.0227199948T^2$
298.15–6000	GPYROZR = 4GZRO2C + 93484.8915
298.15–6000	GPYROGD = 2GGD2O3C + 64889.5871
298.15–6000	GPYROGD2 = 2GGD2O3C + 24520.8115
298.15–1000	GHSEROO = $-3480.87 - 25.503038T - 11.136T\ln(T) - 0.005098888T^2 + 6.61846 \times 10^{-7}T^3 - 38365/T$
1000–3300	$-6568.763 + 12.65988T - 16.8138T\ln(T) - 5.95798 \times 10^{-4}T^2 + 6.781 \times 10^{-9}T^3 + 262905/T$
3300–6000	$-13986.728 + 31.259625T - 18.9536T\ln(T) - 4.25243 \times 10^{-4}T^2 + 1.0721 \times 10^{-8}T^3 + 4383200/T$
298.15–2128	GHSERZR = $-7827.595 + 125.64905T - 24.1618T\ln(T) - 0.00437791T^2 + 34971/T$
2128–6000	$-26085.921 + 262.724183T - 42.144T\ln(T) - 1.342895 \times 10^{31}T^{-9}$
298.15–1000	GHSERGD = $-6834.5855 + 97.13101T - 24.7214131T\ln(T) - .002852405521T^2 - 3.14674076 \times 10^{-7} T^3 - 8665.73348/T$
1000–1508.15	$-6483.25362 + 95.6919924T - 24.6598297T\ln(T) - 0.00185225011T^2 - 6.61211607 \times 10^{-7}T^3$
1508.15–3600	$-123124.992 + 699.125537T - 101.800197T\ln(T) + 0.01506442246T^2 - 6.39165948 \times 10^{-7}T^3 + 29356890.3/T$
298.15–700	GHSERAL = $-7976.15 + 137.071542T - 24.3671976T\ln(T) - 0.0018846662T^2 - 8.77664 \times 10^{-7}T^3 + 74092/T$
700–933.6	$-11276.24 + 223.02695T - 38.5844296T\ln(T) + 0.0185319822T^2 - 5.764227 \times 10^{-6}T^3 + 74092/T$
933.6–2900	$-11277.683 + 188.661987T - 31.748192T\ln(T) - 1.234264\ 10^{28}T^{-9}$

expressed as:

$$\Delta G^{\mathrm{ex}} = \sum_{s} Y_i^s Y_j^s L_{i,j}^s$$

where

$$L_{i,j}^{\mathrm{s}} = \sum_{n} (Y_i^{\mathrm{s}} - Y_j^{\mathrm{s}})^n L_{i,j},$$

are the binary interaction parameters in the sublattice *s*.

In the case of more sublattices (i.e. pyrochlore) the Gibbs energy is expressed by:

$$\Delta G = \sum G_{\mathrm{end}} \prod y_j^s + RT \sum \sum \alpha_s y_j^s + \Delta G^{\mathrm{ex}}$$

where G_{end} is the Gibbs energy of the compound representing the end member. The excess energy for pyrochlore is assumed to be 0.

The liquid phase is described by the partially ionic sublattice model[20] $(Gd^{3+}, Zr^{4+})_P(O^{2-}, Va, AlO_{3/2})_Q$, where P and Q are the number of sites on the cation and anion sublattices, respectively. The stoichiometric factors P and Q vary with the composition in order to maintain electroneutrality.

4. Optimisation

The thermodynamic parameters for the binary systems have been optimised. The thermodynamic data for the Al_2O_3 solid and liquid phases are accepted from work.[25] The thermodynamic data for the Gd_2O_3 solid and liquid phases are available in SGTE database.[26] However the description of SGTE[26] contains unrealistic gaps in heat capacities; the data for the Gd_2O_3 polymorphs and the liquid phase are therefore re-assessed in this study. The C_P data for the Gd_2O_3 cubic phase are from work.[27] The C_P data for Gd_2O_3 monoclinic B phase are re-assessed in this study taking into account data of Knacke et al.[27] and high temperature measurements of enthalpy increment.[28] The same expression of C_P as for B phase was used for the other high-temperature polymorphs of Gd_2O_3. The C_P expression of the liquid phase was assessed in this study by smoothing the SGTE data[26] and checking that liquid phase does not become stable at low temperatures. The enthalpy and entropy of C- and B-Gd_2O_3 are from the reference book of Barin.[29] The enthalpy of B phase at 298 K is in a good agreement with calorimetric measurements.[30] The enthalpies of the transformations for the other polymorphs were calculated using experimental data,[31] the entropy of B $\rightleftarrows$ A, A $\rightleftarrows$ H transformations from work[26] and the entropy of the H $\rightleftarrows$ X transformation assumed to be similar to those of the B $\rightleftarrows$ A and A $\rightleftarrows$ H transformations. The data for the ZrO_2 system are taken to be the same as in work.[21]

The temperature dependence of heat capacity for the $GdAlO_3$ phase was obtained using high-temperature measurements[32] and the value of C_P at 298 K calculated as the sum of C_P for $GdO_{3/2}$ and $AlO_{3/2}$. The data for the GAM phase are accepted from work of Wu and Pelton.[8] Thermodynamic parameters for the Gd_2O_3–Al_2O_3 system have been assessed using calorimetric data[15] and phase equilibrium data.[6–7,9] The GAG phase with garnet structure is not stable in this system. However, the parameters of this metastable phase are assessed using extrapolations of Kanke and Navrotsky,[15] because these data are necessary for high order systems.

The parameters of the ZrO_2–Gd_2O_3 system have been assessed using calorimetric data for the phases with pyrochlore and fluorite structures [16–18,33,34] and phase equilibrium data.[5,35–38]

The system ZrO_2–Al_2O_3 has been assessed by Fabrichnaya et al.[21] However, the parameters of this system have been re-assessed in this study because of the necessity to use other models for the fluorite and tetragonal phases than were used in work.[21] There are no experimental thermodynamic data for this system, that is why only phase equilibrium data have been used in the optimisation.

At the first stage a thermodynamic dataset for the ternary ZrO_2–Gd_2O_3–Al_2O_3 system has been derived by combining the descriptions of the pseudobinary system and assuming ternary interaction parameters to be equal to zero in all phases. The isothermal section at 1473 K has been calculated and compared with the experimental data.[10] It has been found that an agreement of calculated tie-lines with experimental data is possible if the temperatures of invariant reactions (M + Pyr ⇄ F) and (Pyr + C ⇄ F) in the ZrO_2–Gd_2O_3 system are low enough. So far the temperatures of these reactions have not been determined experimentally. Hereby, the phase equilibria in the ternary system constrain the thermodynamic parameters of the binary system.

The liquidus surface and temperatures of invariant reactions in the ternary system have been first calculated with zero ternary interaction parameters in all phases. The results have been compared with experimental estimates of liquidus surface and temperature of the invariant reaction Liq ⇄ AL + F + GAP measured in the present study. In order to get better agreement with the experimental data, ternary interaction parameters have been introduced in the liquid phase description.

5. Results and discussion

The thermodynamic data of the ternary system ZrO_2–Gd_2O_3–Al_2O_3 derived in this study are summarised in Table 1.

5.1. Binary systems

The phase diagram for the $GdO_{3/2}$–$AlO_{3/2}$ system is presented in Fig. 1 along with the available experimental data. The comparison of the calculated and experimental data for invariant reactions in the system is presented in Table 2. The comparison of calculated thermodynamic values with calorimetric data of the $GdO_{3/2}$–$AlO_{3/2}$ system is shown in Fig. 2 and Table 3. According to the calculations, the melting of the GAM phase is incongruent. However, the composition of liquid phase is very close to the composition of the GAM phase.

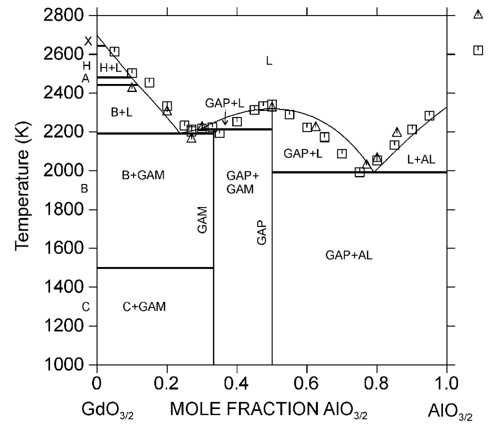

Fig. 1. Phase diagram of the $GdO_{3/2}$–$AlO_{3/2}$ system.

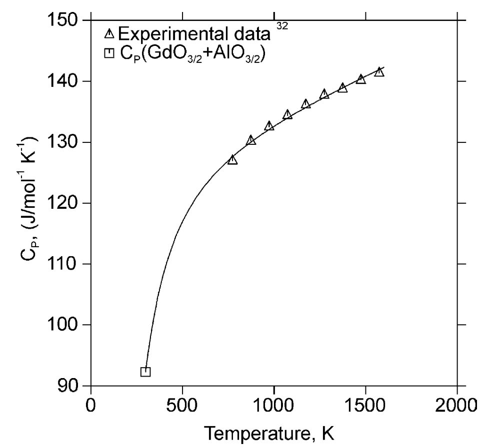

Fig. 2. Calculated heat capacity of the GAP phase along with experimental data.[32]

The calculated phase diagram of the ZrO_2–$GdO_{3/2}$ system is shown in Fig. 3. The comparison of the calculated and experimental data for invariant reactions in the system is given in Table 4. The comparison of calculated thermodynamic values with calorimetric data of the ZrO_2–$GdO_{3/2}$ system is presented in Fig. 4 and Table 5.

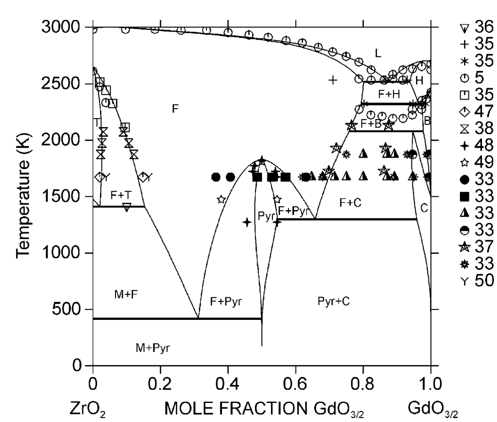

Fig. 3. Phase diagram of the ZrO_2–$GdO_{3/2}$ system.[5,33,35,37,38,47–50]

Table 2
Invariant reactions in the system $GdO_{3/2}$–$AlO_{3/2}$

Reaction and its type	Calculated		Experimental data		
	T (K)	*x* (Liq, $AlO_{3/2}$)	*T* (K)	*x* (Liq, $AlO_{3/2}$)	Reference
L = B + GAM eutectoid	2192	0.237	2203	0.27	[7]
			2163	0.27	[6]
L = GAM congruent			2224		[7]
L = GAM + GAP eutectoid	2213	0.295	2193	0.35	[7]
L + GAP = GAM peritectoid			2223	0.3	[6]
			2175		[9]
L = GAP congruent	2318		2342	0.5	[7]
			2323	0.5	[6]
L = GAP + AL eutectoid	1992	0.791	1993	0.75	[7]
			2020	0.77	[6]

Table 3
Thermodynamic properties of phases in the Gd_2O_3–Al_2O_3 system

T (K)	Property	Calculated	Experimental
977	$\Delta H^{f,ox}$(GAP) $GdO_{3/2} + AlO_{3/2}$ = GAP	−31169	−32330[15]
804	$\Delta H^{r(1)}$ 3GAP + $2AlO_{3/2}$ = GAG	−23780	−23780[15]
2330	ΔH^{melt}(GAP) GAP = L	100432	130000[39]
2220	ΔH^{melt}(GAM) GAM = L	267734	
2213	$\Delta H^{r(2)}$ GAM = L + GAP	213819	166000[9]
298.15–3000	$\Delta G^{f,ox}$(GAM) 4 $GdO_{3/2}$ + $2AlO_{3/2}$ = GAM	−65043 − 6.603T	
298.15–3000	$\Delta G^{f,ox}$(GAG) $3GdO_{3/2}$ + $5AlO_{3/2}$ = GAG	−119771 + 29T	
298.15	$\Delta H^{f,el}$(GAP)	−1785250	
298.15	$\Delta H^{f,el}$(GAM)	−5394530	
298.15	$\Delta H^{f,el}$($Gd_3Al_5O_{12}$)	−7049350	
298.15	S(GAP)	97.402	
298.15	S(GAM)	358.792	
298.15	S(GAG)	324.287	

Reaction (1), $3GdAlO_3 + Al_2O_3 = Gd_3Al_5O_{12}$.
Reaction (2), $Gd_4Al_2O_9 = L + GdAlO_3$.

Table 4
Invariant reactions in the system ZrO_2–$GdO_{3/2}$

Reaction and its type	Calculated		Experimental data		
	T (K)	$x(GdO_{3/2})$	*T* (K)	$x(GdO_{3/2})$	Reference
L = H + X, eutectic	2696	0.9992, 0.9980, 1.0			
L = H + F, eutectic	2516	0.8759, 0.9379, 0.8012	2533	0.867 0.93 0.71	[35]
H + A = B, peritectoid	2455	0.9897, 1.0, 0.9949			
H = B + F, eutectoid	2322	0.9636, 0.9746, 0.7935	2323	0.947 0.802 0.985	[35]
B + F = C, peritectoid	2080	0.9776, 0.7583, 0.9467			
F = Pyr congruent	1825	0.4999	1823	0.50	[40]
T = M + F, eutectoid	1410	0.0203, 0.0, 0.1532	1415		[36]
F = Pyr + C, eutectoid	1298	0.5458, 0.9583, 0.6575			
F = Pyr + M, eutectoid	417	0.4994, 0.0, 0.3124			

Table 5
Calculated and experimental thermodynamic functions

Compositions/function	Experimental data[a]	Calculated results[a]
50 mol% $GdO_{3/2}$, Pyr/ΔH^{0fox}(298) (J/mol)	−13050 ± 1200[16], −25500[41]	−12162
50 mol% $GdO_{3/2}$, F/ΔH^{0fox}(298) (J/mol)	−19000 ± 2000[42]	−8060
45.57 mol% $GdO_{3/2}$, Pyr/ΔH^{0fox}(298) (J/mol)	−12725 ± 825[16]	−9186
53.5 mol% $GdO_{3/2}$, F/ΔH^{0fox}(298), J/mol	−11600 ± 850[16]	−7922
50 mol% $GdO_{3/2}$, Pyr/S^0(298), J/(mol K)	65.85[17]	69.47

Data in work[41] were compiled data from literature.
[a] One mole components (ZrO_2 and $GdO_{3/2}$).

Table 6
Invariant reactions in the system ZrO_2-$AlO_{3/2}$

Reaction and its type	Calculated		Experimental data		
	T (K)	$x(AlO_{3/2})$	T (K)	$x(AlO_{3/2})$	Reference
F = T + L, metatectic	2587	0.0589, 0.0501, 0.3998	2533	0.0952, 0.1308, 0.3333	4
L = T + AL, eutectic	2130	0.7666, 0.0873, 1.0	2183	0.7639, 0.1735, 1.0	43
			2133	0.7730, 0.0952, 1.0	4
			2139	0.7805, 0.0, 1.0	44
			2143	0.7730, 0.0, 1.0	45
			2163	0.7805, 0.0, 1.0	46
T = M + AL eutectoid	1397	0.0258, 0.0, 1.0	1423	0.0198, 0.0, 1.0	4

The calculated phase diagram of the ZrO_2–$AlO_{3/2}$ system is presented in Fig. 5. The calculated data for invariant reactions are compared with experimental data in Table 6.

5.2. The ternary system

Two isothermal sections at 1250 and 1650 °C were constructed according to the XRD results (Fig. 6a and b). They are similar but differ in the details of the phase field GAP + F. The composition of F phase ranges from 28 to 57 mol% $GdO_{3/2}$ at 1650 °C. At 1250 °C, the superstructure Pyr becomes stable in the system ZrO_2–$GdO_{3/2}$ and it wedges into the two-phase field GAP + F by forming three additional fields: GAP + Pyr and two GAP + Pyr + F fields. The isothermal section at 1250 °C is similar to that at 1200 °C studied by other authors.[10] The calculated isothermal sections at 1250 and 1650 °C are presented in Fig. 6c and d. They are in plausible agreement with the experimental results obtained in this study. Calculations at 1200 °C agree well with results of Leckie and Levi.[10] It can be noticed that if pyrochlore phase is in contact with Al_2O_3, a phase with perovskite structure (GAP) forms. This makes it impossible to use the pyrochlore phase as thermal barrier coating on Al_2O_3 (TGO), since pyrochlore and perovskite have different thermal expansion causing cracking. However, the pyrochlore phase could be used as the outer layer of TBC to avoid its direct contact with Al_2O_3. According to the calculations if the ternary interaction parameter is equal to 0 in the liquid phase, liquid becomes stable at 1923 K. Experiments conducted in this study however demonstrate that liquid is not stable at this temperature. Introducing the ternary interaction parameter into the description of the liquid phase suppresses its formation at this temperature. Fig. 6d shows isothermal section at 1923 K calculated taking into account ternary interaction in liquid.

The liquidus surface of the ZrO_2–$GdO_{3/2}$–$AlO_{3/2}$ system was constructed on the base of DTA, petrographic,

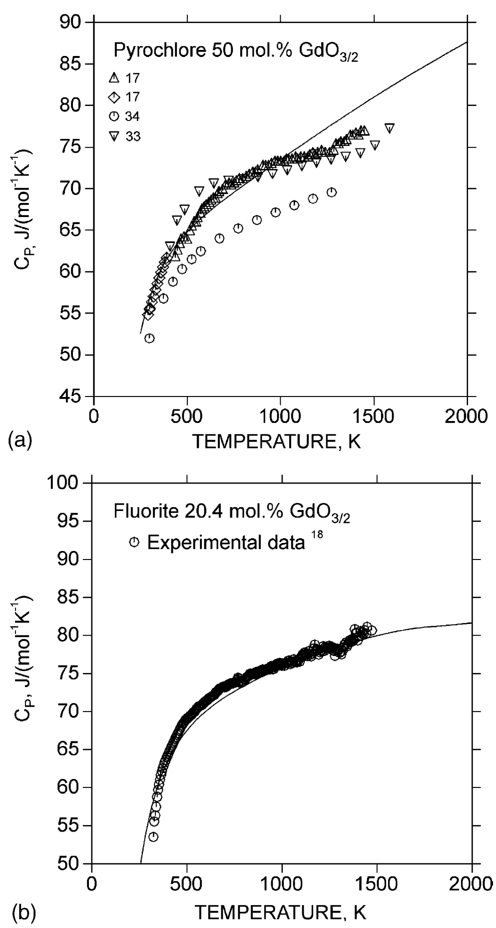

Fig. 4. Calculated heat capacity for pyrochlore (a) and fluorite phase (b) per mole of components ($ZrO_2 + GdO_{3/2}$) along with experimental data.[17–18,33–34]

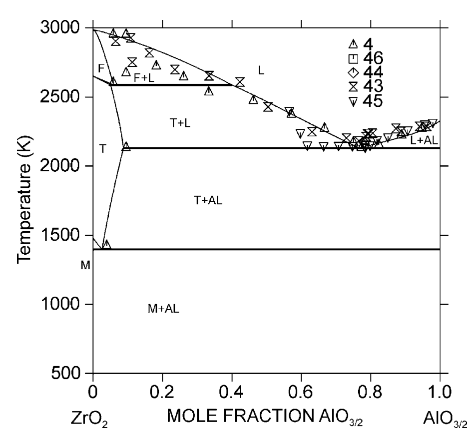

Fig. 5. Phase diagram for the ZrO_2–$AlO_{3/2}$ system.

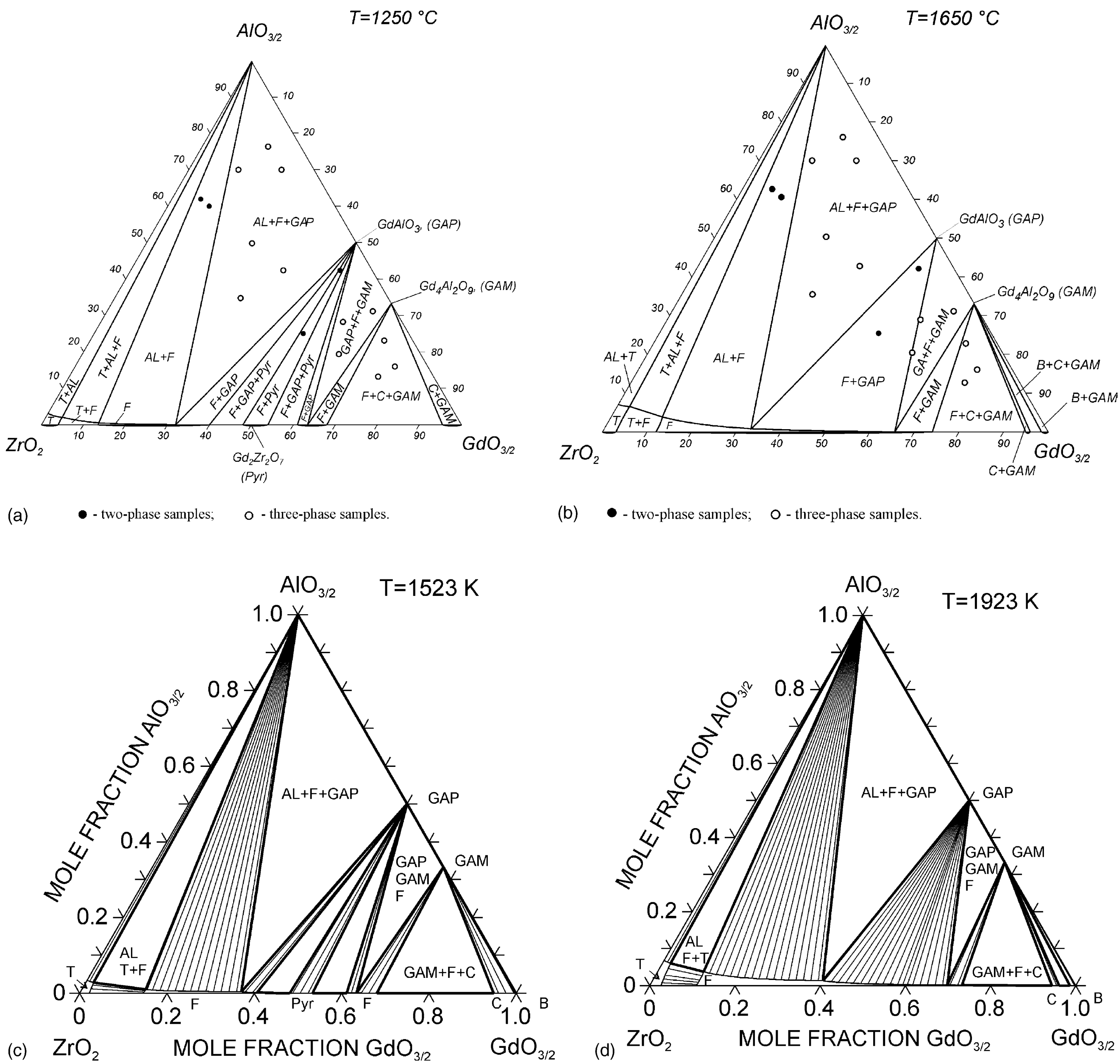

Fig. 6. Isothermal sections of the ZrO_2–$GdO_{3/2}$–$AlO_{3/2}$ phase diagram: (a) experimental data at 1250 °C; (b) experimental data at 1650 °C, ●, two-phase samples; ◯, three-phase samples (c) calculation at 1250 °C, (d) calculations at 1650 °C based on the liquid description containing ternary interaction parameter.

microstructural phase analysis and optimisation data. Petrographic analyses revealed primary phases in the samples. The microstructures of some invariant points are shown in Fig. 7a–d. The phase description is given in the legends to Fig. 7. Eutectics E_1 and E_2 demonstrate a conglomerate phase structure only. Eutectic e3 (saddle point) has an ordinary binary eutectic structure. In the Fig. 7d one can see cellular structure of the ternary eutectic AL + GAP + GAP (E_3). The conclusion that cooperative eutectic growth takes place in this case can be made. The liquidus surface derived from experimental data is presented in Fig. 8a. No new phases and remarkable solid solution areas on the base of components and binary compounds were found in the ZrO_2–$GdO_{3/2}$–$AlO_{3/2}$ system. The liquidus surface consists of nine fields for primary crystallization. The largest liquidus area is occupied by Gd_2O_3 solid solutions in ZrO_2 and is restricted by the envelope $e_{10}U_3E_3e_8E_1e_9E_2U_2e_4$. This field is divided into two primary crystallization fields for solid solutions with fluorite-like cubic (F) and tetragonal (T) structures by the univariant line e_3U_3 ($F \rightleftarrows T + L$). The monoclinic form of ZrO_2 has no primary crystallization field on the liquidus because it exists at temperatures that are below binary and ternary eutectics. The ZrO_2 solid solutions in Gd_2O_3 with X, H, A and B structures of rare earth oxides have their own

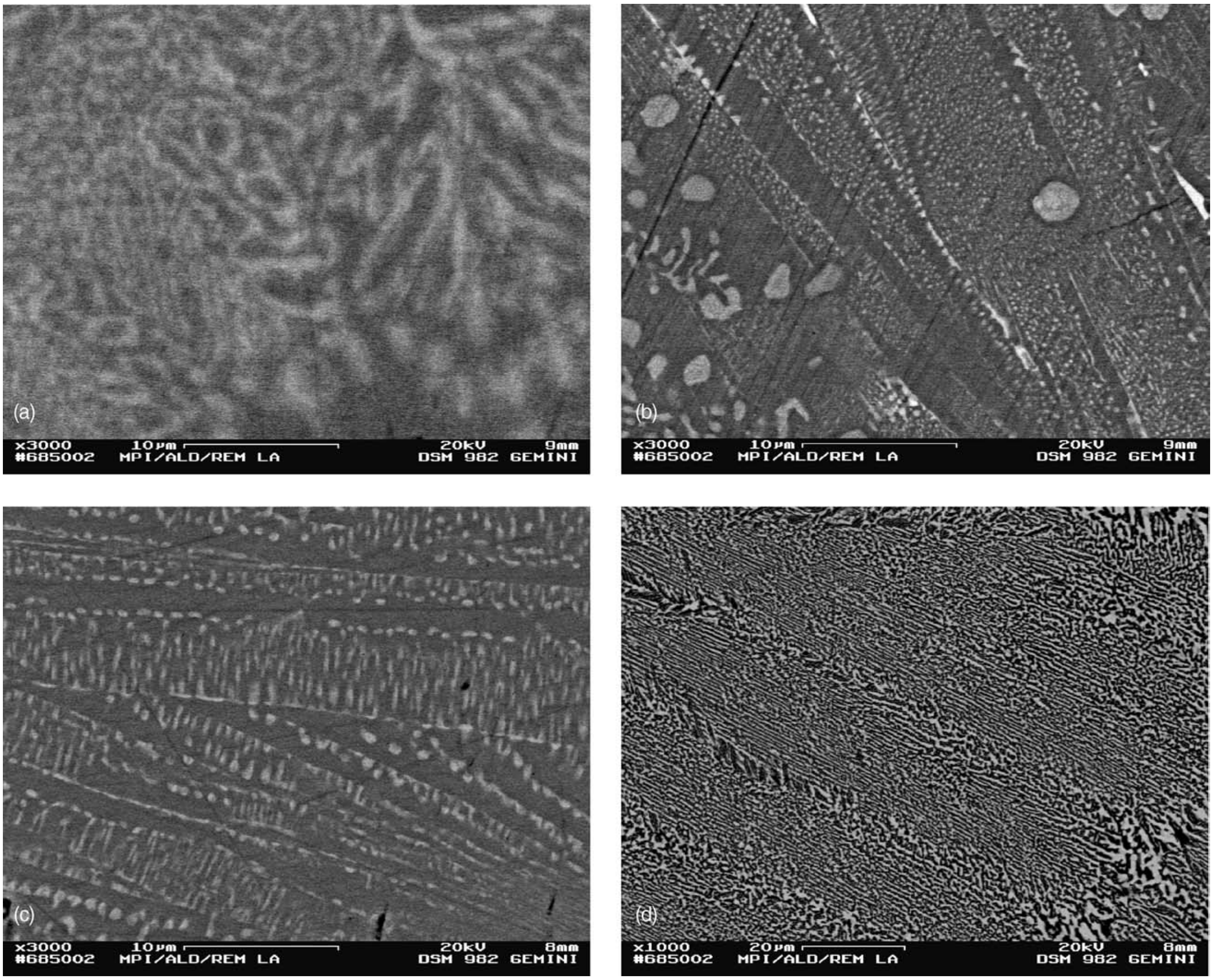

Fig. 7. The microstructures of some alloys in the ZrO_2–$GdO_{3/2}$–$AlO_{3/2}$ system cooled down from melt, mol% (a) Saddle point, $10ZrO_2 + 50GdO_{3/2} + 40AlO_{3/2}$ (e_8): white phase, F; dark phase, GAP. (b) Ternary invariant point, $7ZrO_2 + 71GdO_{3/2} + 28AlO_{3/2}$ (E_2): fine white phase, F; coarse white phase, B, dark matrix, GAM; (c) Ternary invariant point, $7ZrO_2 + 65GdO_{3/2} + 22AlO_{3/2}$ (E_1): fine white phase, F; coarse white phase, GAP; dark matrix, GAM; (d) Ternary invariant point $12ZrO_2 + 21GdO_{3/2} + 67AlO_{3/2}$ (E_3): white phase, F; grey phase, GAP, black phase, AL.

Table 7
Invariant reaction in the system ZrO_2–Gd_2O_3–Al_2O_3

Reaction, type	Calculations with set 1		Calculations with set 2		Experimental data, this work	
	T (K)	Liquid composition $x(GdO_{3/2})$, $x(AlO_{3/2})$	T (K)	Liquid composition $x(GdO_{3/2})$, $x(AlO_{3/2})$	T (K)	Liquid composition $x(GdO_{3/2})$, $x(AlO_{3/2})$
L + A ⇆ H + B, U_1	2455	0.889, 0.110	2455	0.889, 0.110	2423	0.860, 0.110
L + H ⇆ B + F, U_2	2322	0.825, 0.076	2325	0.823, 0.076	2323	0.825, 0.080
L ⇆ GAP + F, e_8	2125	0.571, 0.306	2142	0.556, 0.318	2151	0.500, 0.400
L ⇆ GAM + F, e_9	2095	0.698, 0.217	2109	0.689, 0.227	2135	0.670, 0.260
L ⇆ GAM + GAP + F, E_1	2095	0.675, 0.234	2109	0.685, 0.230	2133	0.630, 0.310
L ⇆ GAM + B + F, E_2	2093	0.725, 0.197	2104	0.735, 0.194	2103	0.700, 0.230
L + T ⇆ AL + F, U_3	2058	0.059, 0.734	2084	0.047, 0.735	2053	0.110, 0.710
L ⇆ AL + F + GAP, E_3	1858	0.229, 0.654	1934	0.225, 0.691	1935[a]	0.210, 0.670

Set 1, calculations without ternary interactions in liquid.
Set 2, calculations with ternary interactions in liquid.
[a] Temperature have been measured using DTA, the other temperatures are estimated from binary systems and melting experiments.

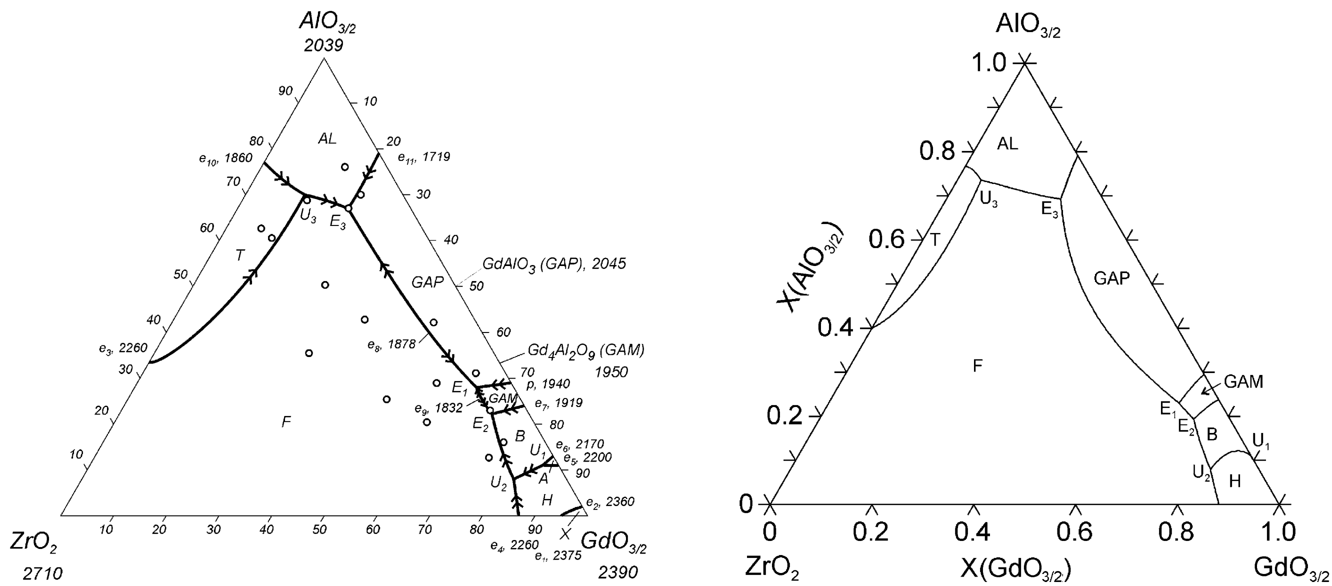

Fig. 8. Projection of the liquidus surface for the system ZrO_2–$GdO_{3/2}$–$AlO_{3/2}$. (a) experimental, (b) calculation.

fields for primary crystallization. As far as high-temperature phases X, H and A cannot be quenched from high temperatures, the coordinates of the respective univariant curves e_1e_2 (X ⇄ H + L), e_5U_1 (H ⇄ A + L), e_6U_1 (A ⇄ B + L), U_1U_2 (H ⇄ B + L) and invariant peritectic points U_1 and U_2 are shown according to the optimisation results. The coordinates of invariant points of the ZrO_2–$GdO_{3/2}$–$AlO_{3/2}$ system are listed in Table 7. The minimum melting temperature in the system is 1662 °C and it corresponds to the ternary eutectic E_3. The maximum liquidus temperature is 2710 °C and it refers to the melting point of pure ZrO_2.

Fig. 8 b shows liquidus surface of the ZrO_2–$GdO_{3/2}$–$AlO_{3/2}$ system calculated using the liquid phase description with a non-zero ternary interaction parameter. The invariant equilibrium data presented in Table 7 were calculated for two datasets with zero and non-zero ternary interaction parameter in the liquid. If the ternary interaction parameter is equal to zero, the agreement of the calculated liquidus surface with experimental estimates is rather good except for the eutectic point E_3 (Liq ⇄ AL + F + GAP). The temperature of the eutectic reaction E_3 was experimentally determined in the present study. The difference between the calculated temperature of this reaction with a zero ternary interaction parameter in the liquid and the experimental value is 77 K. Obviously, including the ternary interaction parameter in the liquid phase improves the thermodynamic description. The temperature of the E_3 eutectic reaction becomes consistent with the DTA measurements while the other reactions remain consistent with estimates based on melting experiments. Some inconsistencies with experimental results still exist for invariant reaction U_3: the calculated temperature is 50 K higher than estimated from experimental data and liquid contains 6% less $AlO_{3/2}$ than follows from petrographic measurements.

The projection of the solidus surface of the ZrO_2–$GdO_{3/2}$–$AlO_{3/2}$ phase diagram is shown in Fig. 9. Data on the composition of solid phases being in three phase equilibria on the solidus surface are obtained from XRD measurements and they are presented in Table 8. According to the liquidus construction, the solidus surface consists of four isothermal three-phase fields corresponding to three invariant equilibrium of the eutectic type and one of the peritectic type. The main solidus area is formed by three isothermal fields AL + F + GAP,

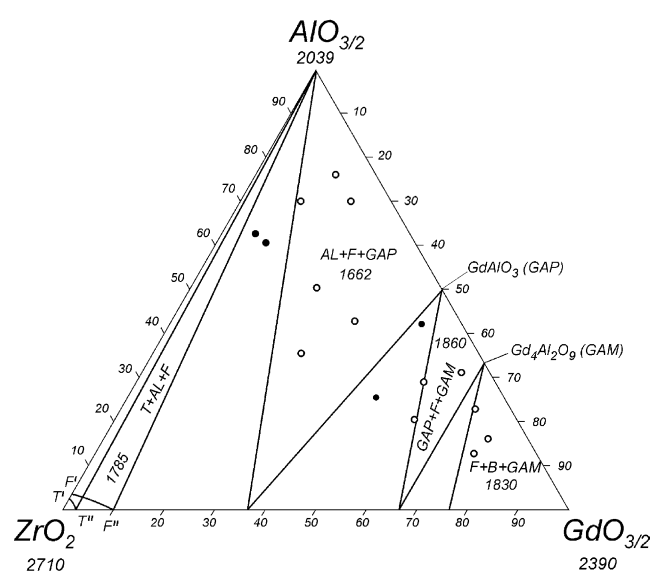

Fig. 9. Projection of the solidus surface for the system ZrO_2–$GdO_{3/2}$–$AlO_{3/2}$. Temperatures (in °C) are for invariant equilibria.

Table 8
Coordinates of the apexes of solid phase tie-line triangles of the solidus surface of the ZrO_2–$GdO_{3/2}$–$AlO_{3/2}$ phase diagram according to the XRD and optimisation data

Phase field	Compositions of equilibrium phases, (mol%)				
	AL	F	GAP	GAM	C
AL + F + GAP	100	63.5 rO_2–36.5 $GdO_{3/2}$	100	–	–
GAP + F + GAM	–	33.5ZrO_2–66.5 $GdO_{3/2}$	100	100	–
GAM + F + B	–	23ZrO_2–77$GdO_{3/2}$	–	100	100

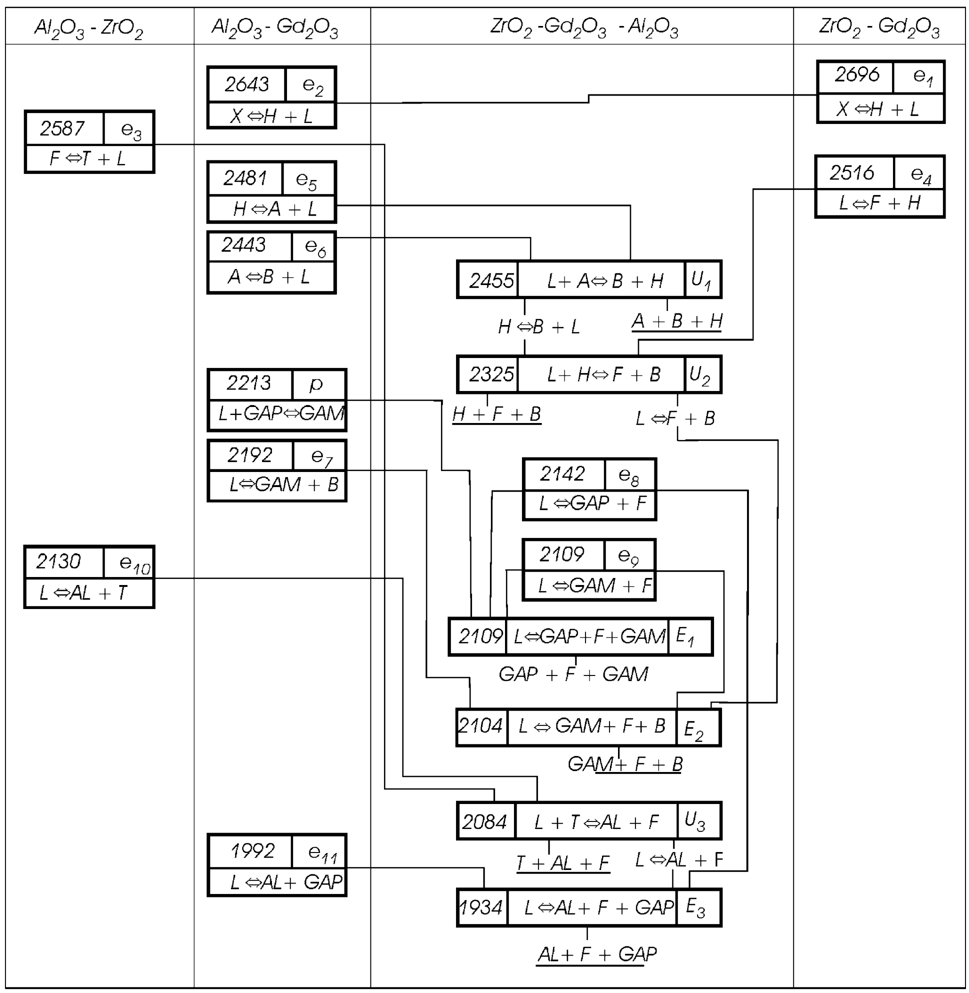

Fig. 10. The Scheil reactions scheme for the ZrO_2–$GdO_{3/2}$–$AlO_{3/2}$ system. Temperatures (K) are given according to the calculations.

GAP + F + GAM and GAM + F + B, which correspond to invariant eutectic equilibria L ⇄ GAM + F + B (E_2, 1830 °C), L ⇄ GAM + F + GAP (E_1, 1860 °C) and L ⇄ AL + F + GAP (E_3, 1662 °C), respectively. The isothermal field T + AL + F corresponds to invariant peritectic equilibrium L + T ⇄ AL + F (U_3, 1785 °C).

Based on the bounding binary systems and on the liquidus and solidus data and the Scheil reaction scheme for the ZrO_2–$GdO_{3/2}$–$AlO_{3/2}$ system has been constructed (Fig. 10). The equilibrium alloys crystallization in this system is characterised by three invariant four-phase transitional reactions at 2150 (U_1), 2050 (U_2), and 1785 °C (U_3), by three invariant four-phase eutectic reactions at 1860 (E_1), 1830 (E_2) and 1662 °C (E_3) and by two maxima on three-phase univariant lines at 1878 (e_8) and 1875 °C (e_9).

6. Conclusions

The phase diagram of the ZrO_2–$GdO_{3/2}$–$AlO_{3/2}$ system was constructed in the temperature range 1250–2800 °C based on experimental studies and thermodynamic optimisation. The liquidus surface of the ternary system reflects the preferentially eutectic character of the reactions. The minimum melting temperature of this system is 1662 °C. It corresponds to the eutectic reaction L ⇄ AL + F + GAP.

The solidus surface projection and the Scheil reaction scheme confirm the preferentially congruent character of phase interaction in the ternary system. No ternary compounds or regions of remarkable solid solubility of Al_2O_3 in the phases were found in the ternary system. The latter observation is promising for creating new ceramics with favourable properties in the ZrO_2–$GdO_{3/2}$–$AlO_{3/2}$ system.

The experimental results obtained in this study have been used to derive a thermodynamic description of the ZrO_2–$GdO_{3/2}$–$AlO_{3/2}$ system. The isothermal sections calculated in the temperature range 1473–1923 K show a good agreement with experimental results obtained in this study and with literature data.[10] The liquidus surface has been calculated. It has been shown that taking a ternary interaction parameter in liquid phase into account makes it possible to bring into agreement experimentally measured and calculated temperature of $L \rightleftarrows AL + F + GAP$ eutectic reaction. However, it is necessary to verify experimentally the temperatures of other invariant reaction beside that of the lowest eutectic.

Acknowledgements

This work was financially supported by HIPERCOAT project of international research collaboration between European Commission (GRD1-2000-30211) and the National Science Foundation USA (DMR-0099685). Authors are thankful to C.G. Levi for fruitful discussions and R. Leckie, R. Mevrel and J. Wu for providing unpublished experimental data.

References

1. Rebollo, N. R., Fabrichnaya, O. and Levi, C. G., Phase stability of Y + Gd co-doped zirconia. *Z. Metallkd.*, 2003, **95**, 163–170.
2. Wu, J., Padture, N. P., Klemens, P. G., Gell, M., Garcia, E., Miranzo, P. *et al.*, Thermal conductivity of ceramics in the ZrO_2–$GdO_{1.5}$ system. *J. Mater. Res.*, 2002, **17**, 3193–3200.
3. Wu, J., Wei, X., Padture, N. P., Klemens, P. G., Gell, M., Garcia, E. *et al.*, Low-thermal-conductivity rare-earth zirconates for potential thermal-barrier-coating application. *J. Am. Ceram. Soc.*, 2002, **85**, 3031–3035.
4. Lakiza, S. M. and Lopato, L. M., Stable and metastable phase relations in the system Alumina–Zirconia–Yttria. *J. Am. Ceram. Soc.*, 1997, **80**, 893–902.
5. Rouanet, A. and Foex, M., Etude a haute temperature des systemes formes par la zircone avec les sesquioxydes de samarium et de gadolinium. *C. R. Acad. Sci.*, 1968, **C267**(15), 873–876.
6. Budnikov, P. P., Kushakovskij, V. I. and Belevantsev, V. S., Investigation of the systems Gd_2O_3–Al_2O_3 and Sm_2O_3. *Dokl. AN SSSR*, 1965, **165**, 1075–1077.
7. Mizuno, M., Yamada, T. and Noguchi, T., Phase diagram of the systems Al_2O_3–Eu_2O_3 and Al_2O_3–Gd_2O_3 at high temperatures. *J. Ceram. Soc. Jpn.*, 1977, **85**(11), 543–548.
8. Wu, P. and Pelton, A. D., Coupled thermodynamic—phase diagram assessment of the rare earth oxide–aluminium oxide binary systems. *J. Alloys Comp.*, 1992, **179**, 259–287.
9. Gervais, M. and Douy, A., Solid phase transformation and melting of the compounds $Ln_4Al_2O_9$ (Ln = Gd, Dy, Y). *Mater. Sci. Eng.*, 1996, **38**, 118–121.
10. Leckie, R. and Levi, C.G., Personal communication.
11. Yokokawa, H., Sakai, N., Kawada, T. and Dokiya, M., Phase diagram calculations for ZrO2 based ceramics: thermodynamic regularities in zirconate formation and solubilities of transition metal oxides. In *Science and Technology of Zirconia V*, ed. S. P. S. Badwal, M. J. Bannister and R. H. J. Hannink. The Australian Ceramic Soc, The Technomic Publ. Co. Inc., Lancaster, PA, 1993, pp. 59–68.
12. Doerner, P., Gauckler, L. J., Krieg, H., Lukas, H. L., Petzow, G. and Weiss, J., On the calculation and representation of multicomponent systems. *Calphad*, 1979, **3**, 241–257.
13. Ball, R. G. J., Mignanelli, M. A., Barry, T. I. and Gisby, J. A., The calculation of phase equilibria of oxide core-concrete systems. *J. Nucl. Mater.*, 1993, **201**, 238–249.
14. Wu, P., *Optimization and Calculation of Thermodynamic Properties and Phase Diagrams of Multicomponent Oxide Systems*. Ph.D. thesis, Ecole Polytechnique, Montreal, Canada, 1992.
15. Kanke, Y. and Navrotsky, A., A calorimetric study of the lanthanide aluminium oxides and the lanthanide gallium oxides: stability of the perovskites and the garnets. *J. Solid State Chem.*, 1998, **141**, 424–436.
16. Helean, K. B., Begg, B. D., Navrotsky, A., Ebbinghaus, B., Weber, W. J. and Ewing, R. C., Enthalpies of formation of $Gd_2(Ti_{2-x}Zr_x)O_7$ pyrochlores. In *Matreials Research Society Symposium Proceedings 663, Scientific Basis for Nuclear Waste Management 24*, 2000, pp. 691–697.
17. Lutique, S., Javorsky, P., Konings, R. J. M., Krupa, J.-C., van Gendern, A. C. G., van Miltenburg, J. C. *et al.*, The low-temperature heat capacity of some lantanide zirconates. *J. Chem. Thermodyn.*, 2004, **36**, 609–618.
18. Mevrel, R., Personal communication.
19. Saunders, N. and Miodovnik, P., *Calphad (Calculation of Phase Diagram: a Comprehensive Guide)*. Pergamon, Oxford, 1998.
20. Hillert, M., The compound energy formalism. *J. Alloys Comp.*, 2001, **320**, 161–176.
21. Fabrichnaya, O. and Aldinger, F., Assessment of thermodynamic parameters in the system ZrO_2–Y_2O_3–Al_2O_3. *Z. Metallkd.*, 2004, **95**, 27–39.
22. Ceder, C., Kohan, A. F., Aydinol, M. K., Tepisch, P. D. and Van der Ven, A., Thermodynamics of oxides with substitutional disorder: a microscopic model and evaluation of important energy contributions. *J. Am. Ceram. Soc.*, 1998, **81**, 517–525.
23. Wilde, P. J. and Catlow, C. R. A., Defects and diffusion in pyrochlore structured oxides. *Solid State Ionics*, 1998, **112**, 173–183.
24. Pirzada, M., Grimes, R. W., Minervini, L., Maguire, J. F. and Sickafus, K. E., Oxygen migration in $A_2B_2O_7$ pyrochlores. *Solid State Ionics*, 2001, **140**, 201–208.
25. Hallstedt, B., Thermodynamic calculation of some subsystems in the Al–Ca–Mg–Si–O system. *J. Phase Equilib.*, 1993, **14**, 662–675.
26. SGTE Substance Database 98SSUB, 1998.
27. Knacke, O., Kubaschewski, O. and Hesselmann, K., *Thermochemical Properties of Inorganic Substances*. Springer-Verlag, Berlin, Heidelberg, 1991.
28. Shpil'rain, E. E., Kagan, D. N., Barkhatov, L. S., Zhmakin, L. I., Koroleva, V. V. and Coutures, J. P., Thermophysical properties of gadolinium oxide in solid phase. *Rev. Int. Hautes Temp. Refract.*, 1980, **17**, 134–136.
29. Barin, I., *Thermochemical Data for Pure Substances*. VCH Weinhem, 1995.
30. Cordfunke, E. H. P. and Konings, R. J. M., The enthalpies of formation of lanthanide compounds III. Ln_2O_3(cr). *Thermochim. Acta*, 2001, **375**, 65–79.
31. Shevchenko, A. V., Nigmanov, B. S., Zaitseva, Z. A. and Lopato, L. M., Interaction of samarium and gadolinium oxides with ytrium oxide. *Inorg. Mater.*, 1986, **22**, 681–685.

32. Kolitsch U., *High-temperature Calorimetry and Phase Analysis in RE_2O_3–Al_2O_3–SiO_2Systems*, Ph.D. thesis, Stuttgart University, Germany, 1995.
33. Wang, Ch., Zinkevich, M., Fabrichnaya, O. and Aldinger, F., Experimental investigation and thermodynamic modeling on the ZrO_2–$GdO_{1.5}$ system. In *Calphad XXXIII Program and Abstracts*, 2004, p. 88.
34. Wu, J., Personal communication.
35. Rouanet, A., Contribution to study of zirconium—oxides systems of lanthanides close to melting point. *Rev. Int. Haures Temp. Refract.*, 1971, **8**, 161–180.
36. Negro, A. and Amato, I., Investigation of zirconia–gadolinia system. *J. Less-Common Met.*, 1972, **26**, 81–88.
37. Scott, H. G., Continuous transition between two structure types in the zirconia-gadolinia system. *J. Raman Spectrosc.*, 1976, **5**, 163–180.
38. Katamura, J., Seki, T. and Sakuma, T., The cubic-tetragonal phase equilibria in the ZrO–R2O3 (R = Y, Gd, Sm, Nd) systems. *J. Phase Equilib.*, 1995, **16**, 315–319.
39. Coutures, J. P., Badie, J. M., Berojan, J., Coutures, J., Flamand, R. and Ruanet, A., Stability and thermodynamic properties of rare earth perovskites. *High Temp. Sci.*, 1980, **13**, 331–336.
40. Moriga, T., Yoshiasa, A., Kanamara, F., Koto, K., Yoshimura, M. and Somiya, S., Crystal structure analyses of pyrochlore- and fluorite-type $Zr_2Gd_2O_7$ and anti-phase domain structure. *Solid State Ionics*, 1989, **31**, 319–328.
41. Reznitskii, L. A., Entropy change in the coordination number of zirconium ion and Gibbs energy of formation of rare-earth zirconates. *Inorg. Mater.*, 1995, **31**, 531–532.
42. Korneev, V. R., Glushkova, V. N. and Keler, E. K., Heat of formation of rare-earth zirconates. *Inorg. Mater.*, 1971, **7**, 781–782.
43. Fischer, G. R., Manfredo, L. J., McNally, R. N. and Doman, R. C., The eutectic and liquidus in the Al_2O_3–ZrO_2 system. *J. Mater. Sci.*, 1981, **16**, 3447–3451.
44. Alper, A. M., Doman, R. C., McNally, R. N. and Yeh, H. C., The use of phase diagrams in fusion-cast refractory materials research. *Phase Diagrams*. Acad. Press, London, New York, 1970, pp. 117–146.
45. Jerebtsov, D. A., Mikhailov, G. G. and Sverdina, S. V., Phase diagram of the system Al_2O_3–ZrO_2. *Ceram. Int.*, 2000, **26**, 821–823.
46. Schmid, F. and Viechnicki, D., Oriented Eutectic Microstructures in the system Al_2O_3/ZrO_2. *J. Mater. Sci*, 1970, **5**, 470–473.
47. Leung, D. K., Chan, C.-J., Ruehle, M. and Lange, F. F., Metastable crystallization, phase partitioning, and grain-growth of ZrO_2–Gd_2O_3 materials processed from liquid precursors. *J. Am. Ceram. Soc.*, 1991, **74**, 2786–2792.
48. Perez y Jorba, M., Contribution to study of systems of zirconium—reare earth oxides. *Annal Chim. Fr.*, 1962, **7**, 479–511.
49. Karaulov, A. G. and Zoz, E. I., Phase formation in the ZrO_2–HfO_2–Gd_2O_3 and ZrO_2–HfO_2–Yb_2O_3 systems. *Refract. Ind. Ceram.*, 1999, **40**, 479–483.
50. Dutta, S., Bhattacharya, S. and Agrawal, D. C., Electrical properties of ZrO_2–Gd_2O_3 ceramics. *Mater. Sci. Eng.*, 2003, **B100**, 191–198.